NANO LETTERS

2009
Vol. 9, No. 7
2630-2635

Exploiting Collective Effects of Multiple Optoelectronic Devices Integrated in a Single Fiber

Fabien Sorin,[†,‡,§] Ofer Shapira,[‡,§] Ayman F. Abouraddy,[||] Matthew Spencer,[⊥] Nicholas D. Orf,[†,‡,§] John D. Joannopoulos,[§,#] and Yoel Fink[*,†,‡,§]

Department of Materials Science and Engineering, Research Laboratory of Electronics, Institute for Soldier Nanotechnology, Department of EECS, Department of Physics, Massachusetts Institute of Technology, Cambridge, Massachusetts 02139, and CREOL, The College of Optics and Photonics, University of Central Florida, Orlando, Florida 32816

Received March 26, 2009; Revised Manuscript Received May 29, 2009

ABSTRACT

The opportunities and challenges of realizing sophisticated functionality by assembling many nanoscale devices, while covering large areas, remain for the most part unrealized and unresolved. In this work, we demonstrate the successful fabrication of an eight-device cascaded optoelectronic fiber structure in which components down to 100 nm are individually electrically addressed and can operate collectively to deliver novel functionality over large area coverage. We show that a tandem arrangement of subwavelength photodetecting devices integrated in a single fiber enables the extraction of information on the direction, wavelength, and potentially even color of incident radiation over a wide spectral range in the visible regime. Finally, we fabricated a 0.1 square meter single plane fiber assembly which uses polychromatic illumination to extract images without the use of a lens, representing an important step toward ambient light imaging fabrics.

The fabrication of multimaterial fibers involves the construction of macroscale preforms that are subsequently stretched into long (hundreds of meters), thin, flexible, and lightweight fibers that deliver prescribed functionalities.[1] Optical transport,[2,3] external reflection,[4] lasing,[5] but also optical[6−8] and thermal[9] detection can be achieved in fibers integrating a judicious choice of materials, engineered in a proper structure. This renders these fibers systems a compelling candidate for applications such as remote and distributed sensing, large-area optical-detection arrays, and functional fabrics.[1,6−9] A limitation of these novel fiber devices, however, has been the challenge of integrating multiple optoelectronic components into a single fiber cross-section. This is in fact a common problem in nanotechnology where the drive toward smaller and smaller nanoscale devices complicates the ability to integrate and individually address many of them, especially over very large-area coverage. Integration of multiple devices to work collectively is however key to the delivery of complex functionality.

The fabrication process described here demonstrates that this limitation can be overcome in polymer fibers. We show that ordered, independent, and globally oriented nanometer scale devices of unprecedented aspect ratio can be integrated within lightweight and flexible fiber substrates that can potentially cover and functionalize very large surface areas (several square meters) and fabric systems.

The fiber integrated devices presented here consist of a pair of metallic electrodes contacting a semiconducting ring that extends along the entire fiber axis, as depicted in Figure 1. Several such pairs can be placed along the ring circumference, and multiple successive rings can be cascaded in the radial direction, forming an integrated system of increasing device density. Schematic diagrams in Figure 1a depict the different steps we developed to produce a preform of two embedded semiconductor rings, each contacted by four electrodes. A series of polymer tubes having precise dimensions so that they fit tightly into each other are fabricated. Thin layers of semiconducting film of prescribed thickness are thermally deposited on a polymer substrate and rolled onto specific tubes. The set of tubes and semiconductor films are then stacked together to form the macroscopic preform. After thermal consolidation under vacuum, the preform is thermally drawn into a fiber that preserves the original cross-

* To whom correspondence should be addressed. E-mail: yoel@mit.edu.
[†] Department of Materials Science and Engineering, Massachusetts Institute of Technology.
[‡] Research Laboratory of Electronics, Massachusetts Institute of Technology.
[§] Institute for Soldier Nanotechnology, Massachusetts Institute of Technology.
[||] University of Central Florida.
[⊥] Department of EECS, Massachusetts Institute of Technology.
[#] Department of Physics, Massachusetts Institute of Technology.

10.1021/nl9009606 CCC: $40.75
Published on Web 06/15/2009

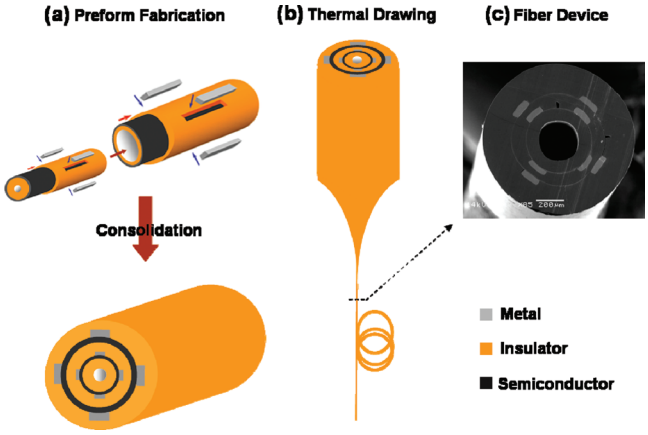

Figure 1. (a) Schematics of the fabrication steps of a preform containing two thin-films at prescribed radial position, each contacted by four metallic electrodes. (b) Schematic of the preform-to-fiber thermal drawing approach. (c) SEM micrograph of the resulting fiber cross-section, illustrating the uniform conservation of the cross-section structure from the macroscopic preform to the microscopic fiber.

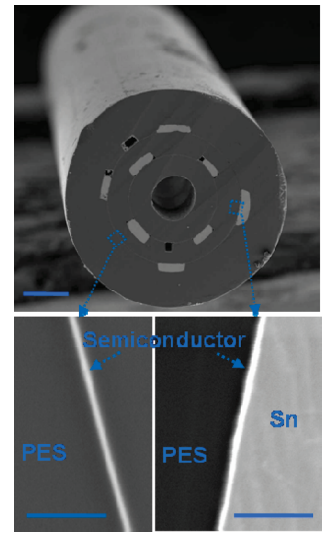

Figure 2. Top: SEM micrographs of a dual-ring fiber where the position of the electrodes contacting the inner layer are rotated by 45° with respect to those contacting the outer layers (scale bar 100 μm). Bottom left: a semiconducting film (scale bar 1 μm). Bottom right: intimate contact between the film and an electrode (scale bar 1 μm).

section uniformly along tens of meters, as shown on the scanning electron microscope (SEM) micrograph in Figure 1c. Here we used semiconducting glasses from the widely investigated As−Se−Te ternary system (specifically $As_{40}Se_{60}$ and $As_{40}Se_{54}Te_6$ (AST)),[10] Sn as the electrodes and polyethersulfone (PES) as the polymer matrix, a set of materials proven to be compatible for codrawing.[7] The details of glass fabrication and thermal drawing are reported elsewhere.[1,7] Note that this fabrication approach allows great flexibility in the number of films to be integrated, their composition, thickness (from a few micrometers down to below 100 nm), and radial position, as well as the number of electrodes and their placement around the film circumference. This is exemplified in Figure 2, in which the precise alignment of the electrodes between layers, the semiconducting film, and the intimate contact between the semiconductor and an electrode are shown. It is apparent that the film surface roughness is more pronounced at the metal interface, due to the lowest viscosity boundary the glassy layer experiences (the electrode flows as a melt while the polymer is in a high viscosity state during thermal drawing). Moreover, the metallic electrodes are typically tens of micrometers in size which renders trivial electrical contact of each individual device. The film is however uniformly maintained down to below 100 nm in thickness, illustrating the fine level of control over the fiber cross-sectional structure that can be achieved.

This prescribed arrangement of multiple nanometer scale components in a single fiber enables the exploitation of their collective response to impart complex functionalities to fiber devices. This is clearly demonstrated by considering optoelectronic fibers designed for optical detection from any direction and at any point along their entire length.[6−8] Figure 3 illustrates how such fibers with these novel arrangements integrating an increasing number of independent optical detectors can retrieve more and more information about an incoming radiation. We begin with a single semiconducting ring structure as shown in Figure 3a, a system previously studied,[7] but we take an innovative approach that consists of considering each pair of adjacent electrodes contacting the semiconductor as an independent optical detector. By alternatively applying a voltage between one pair at a time, we effectively create four devices, each of which having a different angle of view and hence responding differently to light beams incident at given angles (in the plane defined by the fiber axis). Indeed, for the case represented by the red connection on the schematic of Figure 3a, the electric field in quadrant 1 is stronger than the fields in the other three quadrants. The number of photons absorbed in this quadrant, on which the generated photocurrent depends linearly in the linear regime, will change with the angle of incidence (θ), giving rise to the angular dependence of the normalized photocurrent apparent on the red curve (modeled) and red dots (experimental) in Figure 3a. Here, the theoretical curves were computed using MATLAB by deriving the amount of light absorbed in each quadrant for a wavefront incident in the plane defined by the fiber axis with a given θ. The index of refraction for the polymer and the glass were measured with an ellipsometer and values of 1.6 and 3.2 were used respectively, a good approximation for the range of wavelengths considered. The values of the electric fields were obtained by simulating the structure using the finite element program FEMLAB. The experimental data were recorded using the 514 nm line of an argon ion laser while rotating the fiber around its axis by four degree increments. Note that for this system, the beam polarization had unnoticeable effects on the angular dependence of photogenerated currents.

An illumination event is thus characterized by four current values, from which a unique θ can be extracted. In practice, system noise sets a lower bound on the attainable angular resolution, which depends on many parameters and a

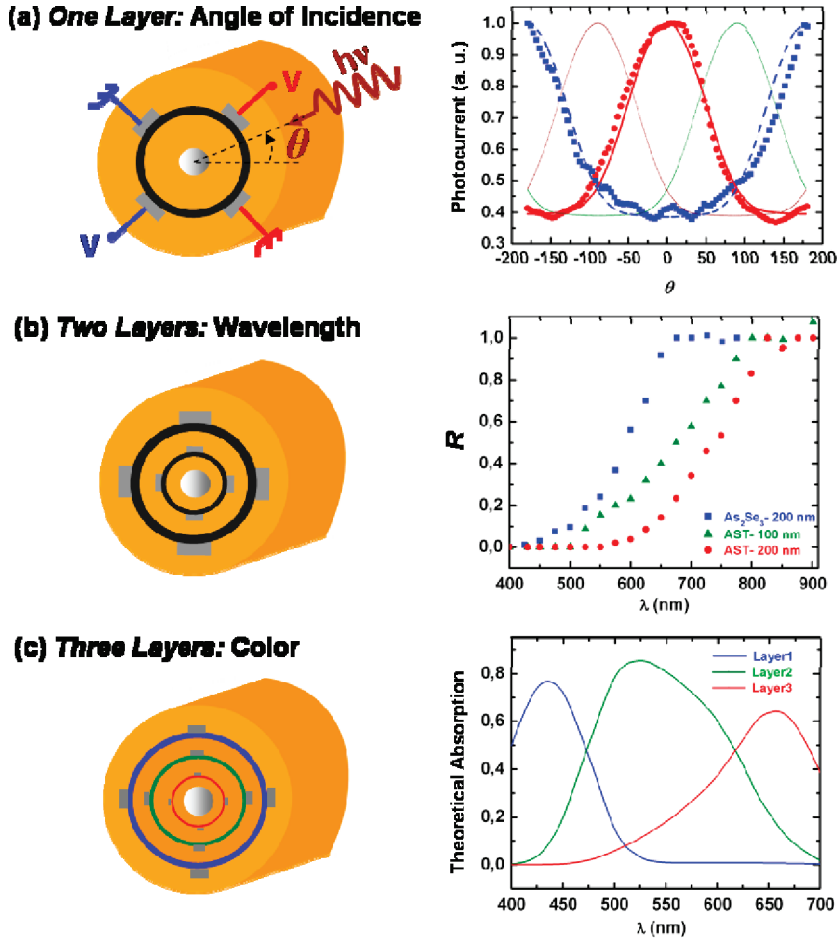

Figure 3. (a) Schematics of a single-layer device, showing connections to adjacent pairs of electrodes. Graph: photocurrent vs angle of incidence. The dots and lines represent the experimental results and the theoretical model, respectively. For clarity we show experimental results for two detectors only. (b) Schematics of a dual-ring structure and graph of the ratio R versus wavelength for fibers made with different glass compositions and thicknesses. (c) Schematic of a three-layer fiber with the graph of the theoretical curves of light absorption for each layer. The curves were multiplied by an appropriate optical filter that block UV and IR signals, which could potentially be integrated in the fiber design.[6]

complete study of it is beyond the scope of this manuscript. To discriminate between two angles of illumination, one needs to take the ratio of the photocurrents generated in two adjacent optical detectors to eliminate the dependence on light intensity. Two angles will be separated if their corresponding current ratios differ more than its associated noise. In our experimental conditions where low intensity illumination was used so that any noise was due only to dark current fluctuations, a resolution down to below 4° was achieved for certain angles of illumination.

This performance can be improved by integration of a second cascaded ring with the configuration shown in Figure 2. Here, eight independent optical detectors, with angle of views shifted by 45° this time, enable the same resolution over a much broader range of incident angles. In this approach however, a limitation comes from the shielding effect of electrodes in the outer layer. For the purpose of angle-of-incidence measurement only, it is preferable to use a single ring configuration with more electrodes and hence with more optical detectors with sharpened angle of views resulting in better resolution. Moreover, cascading devices at different radial positions to operate collectively relies on the partial absorption of the incident radiation in the outer layer. Remarkably, this effect also imparts spectral analysis capabilities to optoelectronic fibers. Consider the simple case of an incident monochromatic beam of unknown wavelength λ and photon flux Φ_0. The photocurrents generated in both layers are proportional to Φ_0 in the linear regime, and depends also on λ through the semiconductor penetration depth ($\delta(\lambda)$) that governs the fraction of photons absorbed in the films (for given film thicknesses).[11,12] These two contributions, however, can be separated due to the information captured by two cascaded optical detectors, a sophisticated operation that a single ring could not perform. The wavelength of the incident light may be extracted, for example, by taking the ratio of the inner and outer layer photocurrents, $R(\lambda)$, for which the dependence on Φ_0 of both signals cancels out. This is demonstrated experimentally in Figure 3b where we report the measurement of $R(\lambda)$ for three fibers, each having an identical structure but with different glass compositions and film thicknesses t: ($As_{40}Se_{60}$, $t = 200$ nm) in blue, (AST, $t = 200$ nm) in red, and (AST, $t = 100$ nm) in green. We used a monochromator as the light source and measured the ratio of currents for inner and outer

detectors of same angle of view to cancel the dependence on the angle of incidence. It is clear that one can extract λ uniquely from such measurement, over a range of frequencies that can be tuned by engineering the film composition and thickness. Indeed, R starts from zero when all the light is absorbed in the first layer, and increases toward longer wavelengths (and hence larger $\delta(\lambda)$), as more photons reach the inner layer. The addition of tellurium to the glass shifts the optical gap toward lower frequencies,[10] and this moves the rise in R to longer wavelengths compared to $As_{40}Se_{60}$ for a given film thickness, which explains the offset of the blue and red data points observed. Similarly, the thin semiconducting layers are less absorptive than thicker layers of the same composition and let through relatively more high frequency photons, explaining the difference between the green and red data points. Here again, a complete discussion of the wavelength resolution of such systems is beyond the scope of this study. In our experimental conditions, it was found to be limited by the fwhm of the monochromator source (around 15 nm). It is treated using a similar approach as described above for the angle of incidence, and under dark conditions (considering dark current noise only) we evaluate that below 5 nm resolution (corresponding to a $\delta\lambda/\lambda \approx 1\%$) could be achieved.

To spectrally analyze polychromatic radiation with this approach, an increasing number of successive rings are required. For example, two simultaneously incoming monochromatic beams of unknown wavelengths and photon flux can be analyzed by a four-ring structure. If the wavelengths are known, however, a dual-ring configuration could separate the a-priori unknown contributions of the two beams, an interesting property we demonstrate and will use below. Intriguingly, the addition of a third layer as depicted in Figure 3c can impart RGB color discrimination to fiber devices. As a proof of concept, we show the theoretical absorption curves for a range of wavelengths in the visible of a three layer system comprising a 400 nm thick outside layer of $As_{40}S_{60}$ glass, (material compatible with our processing technique[5]), a 100 nm thick middle layer of $As_{40}Se_{60}$ and a 300 nm thick inner layer of AST. We used data on the imaginary part of the index of refraction of each material measured with an ellipsometer. From this value the penetration depth can be extracted and the amount of photons absorbed in each film calculated. RGB color discrimination can be achieved with these structures as demonstrated by similar designs in color pixel technology.[13,14]

The remarkable increase in functionality of polymer fibers integrating novel arrangements of nanometer devices is best exploited when one considers the potential coverage area of these systems and the opportunities associated with their assemblies into constructs and fabrics.[1,6−9] In Figure 4, we demonstrate how a single wavelength discriminating fiber web can image a complex object with polychromatic light, noninterferometrically and without lenses, by taking an intensity measurement at a single diffraction plane. In doing so we improve on a previous lensless imaging system that required diffraction patterns at two distances Z and Z' from an object illuminated by a monochromatic beam of wavelength λ.[8] An interesting fact encoded in diffraction integrals in the paraxial limit, however, is that the wavelength of radiation λ and the distance from the plane of radiation to the measurement plane Z always appear as a product:[15] $Z\lambda$. Thus, from the point of view of image formation, the diffraction patterns at distances Z and Z' from an object illuminated by (or radiating at) a wavelength λ are identical to those at a distance Z but for two different wavelengths λ and $\lambda' = (Z'/Z)\,\lambda$. Hence, instead of observing the diffraction pattern at one wavelength but two different planes, one could alternatively detect the identical patterns at the same distance Z but with two wavelengths. This has the surprising ramification that one may reconstruct the lensless image of an object using a single planar fiber web, as long as the fibers can discriminate between the contribution of two sufficiently separated wavelengths. As explained above, dual-ring fibers can perform such a task as long as the wavelengths are known. To experimentally verify this approach, we built a 32 by 32 grid using dual-ring fibers, each around 35 cm in length, as depicted in Figure 4a. This construct integrates more than 500 oriented devices (eight in each fiber) with feature sizes down to 100 nm, each individually electrically addressed, covering a 0.1 square meter area. An object (a smiley face), composed of a chrome mask on a glass substrate with a diameter of 800 μm (with features size of 150 μm), was simultaneously illuminated by an argon laser tuned at 514 nm and a Ti:Sapphire laser tuned at 830 nm. We chose to image an object with significantly more complex contours thanks to the better sensitivity of the fibers composing the grid, typically with a noise equivalent power of a few tens of nanowatts.[7] The total input power used was indeed drastically reduced compared to previous imaging experiment[8] with levels down to below 100 mW for each beam. The grid was first calibrated by uniform illumination of the green and red beams separately, in order to measure the ratio of inner to outer layer currents for each fiber and each beam. The diffraction patterns were measured at 8 cm away from the object and due to space constraints, the images were magnified to fit the dimensions of the grid. Note that in this proof of principle, the grid only captured the first two diffraction orders. The information contained in the lower energy diffraction orders that was lost due to the limited size of the grid explains the absence of the sharp features representing the ring surrounding the eyes and mouth in the reconstructed, compared to the real object. For each diffraction patterns generated at every angle of rotation of the object (increment of 10° used), the fiber grid intercepts a superposition of the diffraction patterns due to the 514 and the 830 nm photons. To understand how one can separate these two contributions and reconstruct the diffraction pattern of each individual wavelength, let us consider a single fiber in the grid on which is simultaneously incident two photon flux Φ and Φ' of distinct wavelengths λ and λ' respectively. Photocurrents are generated in the inner ($I_{in}(\Phi,\Phi')$) and outer layers ($I_{out}(\Phi,\Phi')$), and the contribution of each beam, in the outer layer for example, can be distinguished using the follwing simple formulas: $I_{out}(\Phi,0) = [1/(R' - R)]\text{-}(R'I_{out}(\Phi,\Phi') - I_{in}(\Phi,\Phi'))$, and $I_{out}(0,\Phi') = I_{out}(\Phi,\Phi') -$

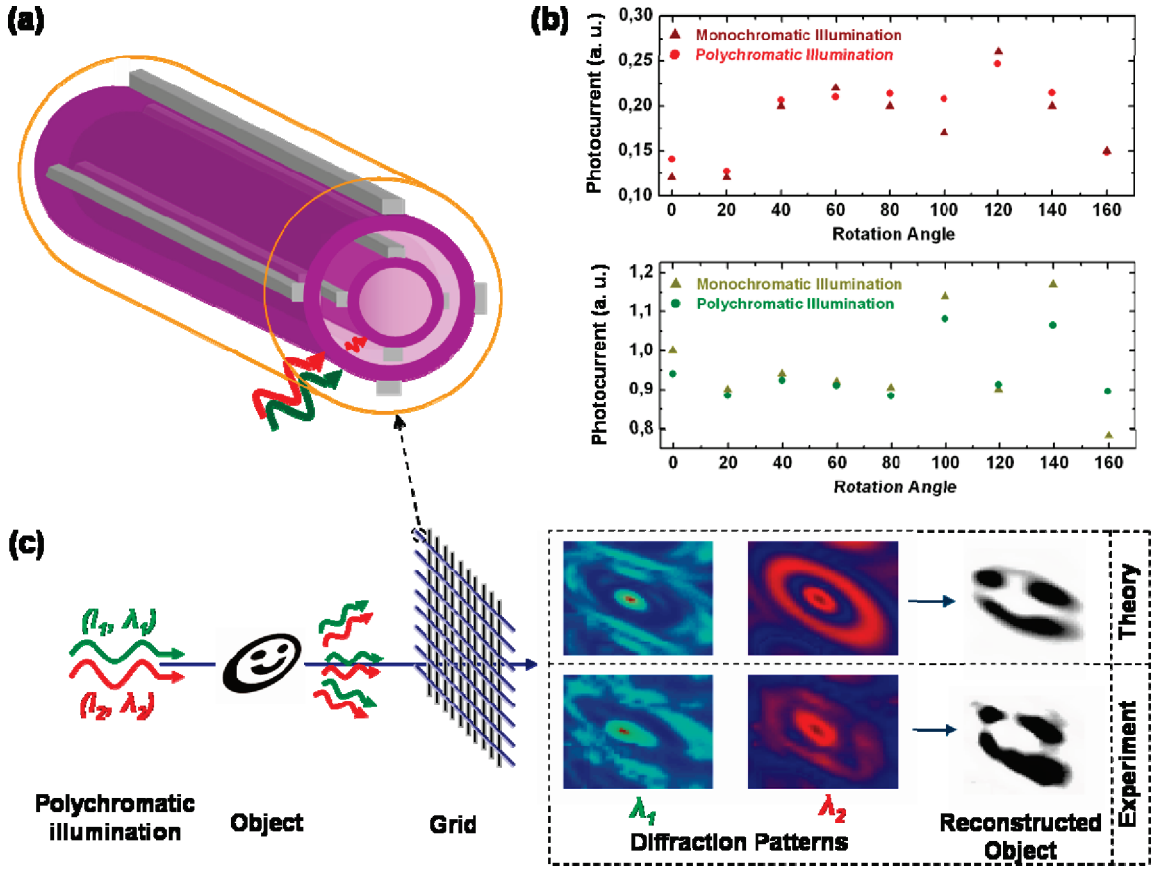

Figure 4. (a) Schematic of the dual-ring fibers forming the grid with the illustration of green and red light reaching the fiber. The schematic is not to scale; the fibers were around 35 cm in length, 800 μm in diameter, and the semiconducting layers around 100 nm in thickness. (b) Experimental data of the currents generated in the outer layer of a fiber in the grid for a few rotations of the object. Green and red triangles are currents measured when the grid is illuminated by the green or red radiation alone, respectively. The dots represent the reconstructed currents from the green (green dots) and the red (red dots) beams when polychromatic radiation is used. (c) Principle of single grid lensless imaging: An object (smiley face) is illuminated by polychromatic radiation. The two diffracted patterns are obtained at the grid location. The phase-retrieval algorithm is used to reconstruct the object. The first row shows theoretical calculations while the second shows the experimental results.

$I_{out}(\Phi,0)$, where R (respectively R') is the calibrated ratio of the current in the inner layer to the one in the outer layer when the fiber is illuminated by a monochromatic beam of wavelength λ (respectively λ'). This result is shown in Figure 4b where we compared the measured photocurrents generated in the outer layer of a fiber illuminated by green (514 nm, top graph) and red (830 nm, bottom graph) monochromatic beams alone with the photocurrents reconstructed using the formula presented above when the fiber is illuminated by the same beams simultaneously. Applying this approach, we could extract the diffraction images of each beam for all angles of rotation of the object and apply the back projection algorithm to reconstruct the diffraction patterns of the red and green lights as shown in Figure 4c. The object can then be imaged using the same phase retrieval algorithm and concepts described in previous work.[8]

In conclusion, we demonstrated the fabrication of meters long, lightweight, and flexible fibers, integrating up to eight optical detectors with feature sizes down to 100 nm, using simple and inexpensive thermal drawing techniques. A dual ring architecture was fabricated leading to wavelength discrimination in the visible at below 5 nm resolution. A similar design was used to measure angle of incidence down to 4° angular resolution. A single planar grid of wavelength sensitive fibers was assembled and used to demonstrate lensless imaging with polychromatic illumination. These results mark a significant step for the emerging technology platform of multimaterial fibers integrating nanometer size devices that are capable of complex functionalities over very large area systems and fabrics.

Acknowledgment. This work was supported by ARO-ISN, DARPA and DOE. This project was also supported in part by the MRSEC program of the NSF. We also thank RLE for its support. The authors thank Dursen Saygin-Hinczewski, Dr. Sylvain Danto, Dr. Shandon D. Hart and Dr. Ismaila Dabo for their help at different stages of the project.

References

(1) Abouraddy, A. F.; Bayindir, M.; Benoit, G.; Hart, S. D.; Kuriki, K.; Orf, N.; Shapira, O.; Sorin, F.; Temelkuran, B.; Fink, Y. *Nat. Mater.* **2007**, *6*, 336–347.
(2) Temelkuran, B.; Hart, S. D.; Benoit, G.; Joannopoulos, J. D.; Fink, Y. *Nature* **2002**, *420*, 650–653.
(3) Kuriki, K.; Shapira, O.; Hart, S. D.; Benoit, G.; Kuriki, Y.; Viens, J.; Bayindir, M.; Joannopoulos, J. D.; Fink, Y. *Opt. Express* **2004**, *12*, 1510–1517.
(4) Hart, S. D.; Maskaly, G. R.; Temelkuran, B.; Prideaux, P. H.; Joannopoulos, J. D.; Fink, Y. *Science* **2002**, *282*, 1679–1682.

(5) Shapira, O.; Kuriki, K.; Orf, N.; Abouraddy, A. F.; Benoit, G.; Viens, J.; Rodriguez, A.; Ibanescu, M.; Joannopoulos, J. D.; Fink, Y. *Opt. Express* **2006**, *14*, 3929–3935.
(6) Bayindir, M.; Sorin, F.; Abouraddy, A. F.; Viens, J.; Hart, S. D.; Joannopoulos, J. D.; Fink, Y. *Nature* **2004**, *431*, 826–829.
(7) Sorin, F.; Abouraddy, A. F.; Orf, N.; Shapira, O.; Viens, J.; Arnold, J.; Joannopoulos, J. D.; Fink, Y. *Adv. Mater.* **2007**, *19*, 3872–3877.
(8) Abouraddy, A. F.; Shapira, O.; Bayindir, M.; Arnold, J.; Sorin, F.; Hinczewski, D. S.; Joannopoulos, J. D.; Fink, Y. *Nat. Mater.* **2006**, *5*, 532–536.
(9) Bayindir, M.; Abouraddy, A. F.; Joannopoulos, J. D.; Fink, Y. *Adv. Mater.* **2005**, *18*, 845–849.
(10) Borisova, Z. U. *Glassy Semiconductors*; Plenum Press: New York, 1981.
(11) Rosencher E.; Vinter B. *Optoelectronics*; Cambridge University Press: Cambridge, 2002.
(12) Sze, S. M. *Semiconductor Devices: Physics and Technology*, 2nd ed.; John Wiley: New York, 2001.
(13) Lyon, R. F.; Hubel; P. M. *Eyeing the Camera: into the Next Century*; 10th Color Imaging Conference: Color Science and Engineering Systems, Technologies, Applications, Scottsdale, Arizona; November 12, 2002; pp 349−355.
(14) Knipp, D.; Street, R. A.; Stiebig, H.; Krause, M.; Lu, J.; Ready, S.; Ho, J. *Opt. Express* **2006**, *14*, 3106–3113.
(15) Saleh, B. E. A.; Teich, M. C. *Fundamentals of Photonics*; John Wiley: New York, 1991.

NL9009606